JACS
JOURNAL OF THE AMERICAN CHEMICAL SOCIETY

ARTICLE

pubs.acs.org/JACS

Manganese Triazacyclononane Oxidation Catalysts Grafted under Reaction Conditions on Solid Cocatalytic Supports

Nicholas J. Schoenfeldt,[†] Zhenjuan Ni,[‡] Andrew W. Korinda,[†] Randall J. Meyer,[‡] and Justin M. Notestein*[,†]

[†]Department of Chemical and Biological Engineering, Northwestern University, 2145 Sheridan Road, Technological Institute, Room E136, Evanston, Illinois 60208, United States

[‡]Department of Chemical Engineering, University of Illinois at Chicago, 810 South Clinton Street, Chicago, Illinois 60607, United States

Supporting Information

ABSTRACT: Manganese complexes of 1,4,7-trimethyl-1,4,7-triazacyclononane (tmtacn) are highly active and selective alkene oxidation catalysts with aqueous H_2O_2. Here, carboxylic acid-functionalized SiO_2 simultaneously immobilizes and activates these complexes under oxidation reaction conditions. H_2O_2 and the functionalized support are both necessary to transform the inactive $[(tmtacn)Mn^{IV}(\mu\text{-}O)_3Mn^{IV}(tmtacn)]^{2+}$ into the active, dicarboxylate-bridged $[(tmtacn)Mn^{III}(\mu\text{-}O)(\mu\text{-}RCOO)_2Mn^{III}(tmtacn)]^{2+}$. This transformation is assigned on the basis of comparison of diffuse reflectance UV−visible spectra to known soluble models, assignment of oxidation state by Mn K-edge X-ray absorption near-edge spectroscopy, the dependence of rates on the acid/Mn ratios, and comparison of the surface structures derived from density functional theory with extended X-ray absorption fine structure. Productivity in *cis*-cyclooctene oxidation to epoxide and *cis*-diol with 2−10 equiv of solid cocatalytic supports is superior to that obtained with analogous soluble valeric acid cocatalysts, which require 1000-fold excess to reach similar levels at comparable times. Cyclooctene oxidation rates are near first order in H_2O_2 and near zero order in all other species, including H_2O. These observations are consistent with a mechanism of substrate oxidation following rate-limiting H_2O_2 activation on the hydrated, supported complex. This general mechanism and the observed alkene oxidation activation energy of 38 ± 6 kJ/mol are comparable to H_2O_2 activation by related soluble catalysts. Undesired decomposition of H_2O_2 is not a limiting factor for these solid catalysts, and as such, productivity remains high up to 25 °C and initial H_2O_2 concentration of 0.5 M, increasing reactor throughput. These results show that immobilized carboxylic acids can be utilized and understood like traditional carboxylic acids to activate non-heme oxidation catalysts while enabling higher throughput and providing the separation and handling benefits of a solid catalyst.

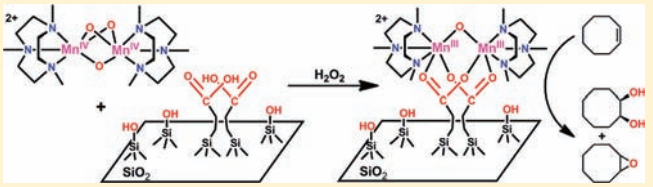

1. INTRODUCTION

The oxidation of alkenes yields reactive chemical intermediates such as epoxides and vicinal diols, which are subsequently used in end products such as pharmaceuticals and fine chemicals, polycarbonates, and ethers and glycols.[1] While there are many known routes to these intermediates, there is an increasing demand for environmentally friendly processes using atom-efficient oxidants such as H_2O_2, which in turn require highly active and selective catalysts. Ideally, the catalysts themselves are synthesized from abundant and relatively benign atoms.[2] Mn is a good candidate, as it is the second most abundant transition metal found in the Earth's crust and is utilized in natural enzymes. In general, its accessible oxidation states from +2 to +7 make it ideal for redox catalysis.

Diverse ligands have been developed for use in Mn oxidation catalysis, including salen and porphyrin-type ligands.[3] Equally important are the non-heme-type ligands such as 1,4,7-trimethyl-1,4,7-triazacyclononane (tmtacn)—its Mn complex **1** has been shown to be an active, homogeneous catalyst or precatalyst for low-temperature, selective oxidation with aqueous H_2O_2 on a wide range of substrates.[4] Mn complexes of this ligand first attracted attention as potential models of non-heme metal oxide enzyme active sites, such as in catalase[5] or the water-oxidizing center in photosystem II.[6] Further investigation into the oxidation reactivity of **1** led to a number of reports of activity toward alcohol oxidation,[7] epoxidation and *cis*-dihydroxylation of alkenes,[4] alkane activation,[8] and sulfoxidation.[9] The complex has also been used industrially as a bleaching agent[10] and washing detergent additive[4b] due to its ability to oxidize a wide range of substrates at ambient and below in aqueous and nonaqueous media,[4b,10a] but low selectivity led to its removal from the market.[11]

Alone, complex **1** gives low oxidation yields but consumes H_2O_2, likely via catalysis by a decomposition product of the complex. This so-called catalase activity was found to be greatly reduced by lowering the reaction temperature, maintaining low H_2O_2 concentrations by slow oxidant addition,[4c,10,12] and particularly through the use of carboxylic acid additives, which were also found to control productivity and selectivity in alkene

Received: May 24, 2011
Published: October 04, 2011

oxidation.[7b,13] Subsequent investigations combining complex **1** with carboxylic acids implicated species **2b**, with two bridging carboxylates, as a catalyst resting state or an immediate precursor to the active catalyst. This species formed during induction periods, which could be minimized by combining H_2O_2, **1**, and the carboxylic acid prior to substrate addition, by deliberately synthesizing **2b**, or by using a reducing agent.[14] Mechanistic investigations into epoxidation and *cis*-dihydroxylation over **1** have further implicated activated Mn-hydroperoxides as the active oxidant, although the precise nuclearity and structure of the active intermediate remain subjects of debate.[14,15] The use of this class of catalyst in *cis*-diol synthesis is of particular interest, as catalysts for this transformation are relatively uncommon and can require less-desired species such as OsO_4.[16] In general, there is a need for kinetic investigations into this class of catalyst, in order to determine reaction orders, rate constants, and activation energies that will allow for rational catalyst optimization and would support claims of H_2O- and H_2O_2-dependent pathways involving rate-limiting activation of H_2O_2 at the active site.[14,15]

Recently, we reported that complex **1** can be attached to oxide surfaces, e.g., "heterogenized", under the same conditions in which alkenes are typically oxidized, leading to a simple and effective method for creating an active solid catalyst. The crucial requirement is for the support surface to have been previously functionalized with carboxylic acids.[17] No modification to the triazacyclononane ligand itself is required, in contrast with typical grafting routes, and the stable, easily synthesized complex **1** is used exactly as it would be employed with traditional, soluble carboxylate cocatalysts. Product selectivities are similar to those of the homogeneous catalyst, likely because well-defined surface structures form. In contrast, metalation of previously grafted ligands can lead to unpredictable selectivities and unpredictable or unknown interactions between metal, ligand, surface, and neighboring species.[18] Unusual for heterogenized systems, we also reported productivity increases of up to 9 times for a given quantity of surface-attached carboxylic acids vs the same amount of soluble valeric acid (C_4H_9COOH).[17]

Here we report fully on the synthesis and the alkene oxidation activity/selectivity of **1** heterogenized on carboxylic acid-functionalized SiO_2. We propose the formation of surface complex **2b′**, directly analogous to the proposed active intermediate in soluble systems, based on diffuse reflectance UV−visible spectroscopy, oxidation reactivity as a function of stoichiometry, density functional theory (DFT) models, X-ray absorption near-edge spectroscopy (XANES), and extended X-ray absorption fine structure (EXAFS) data. Reaction orders and apparent activation energies in cyclooctene epoxidation/dihydroxylation by the solid catalyst were determined, allowing the mechanisms of this catalyst to be compared to those of soluble analogues.

2. EXPERIMENTAL METHODS

2.1. Physical Measurements. Solution-phase ^{1}H NMR spectra were recorded on an Inova 500 MHz NMR or an Oxford NMR AS400 spectrometer. Solid-state ^{13}C CP/MAS NMR (adamantane external standard) spectra were recorded on a Varian 400 MHz NMR spectrometer after drying of solid samples at 120 °C under dynamic vacuum. Electrospray ionization mass spectrometry (ESI-MS) was performed on an Agilent 6210 TOF liquid chromatograph/mass spectrometer (LCMS) after dissolving samples in acetonitrile (MeCN). CHN and Mn analyses were performed by Galbraith Laboratories. Thermogravimetric analysis (TGA) was recorded under N_2/O_2 atmosphere using a TA Instruments TGA Q500 instrument in high-resolution mode with a 10 °C/min ramp rate from room temperature to 800 °C. Solution-phase UV−visible spectra were recorded with a Shimadzu UV-3600 UV−vis−NIR spectrophotometer. Diffuse reflectance UV−visible (DRUV) spectra were recorded using a Harrick Praying Mantis attachment. Prior to analysis, supported catalysts were extensively washed with MeCN and vacuum-dried. No attempt at air/moisture-free isolation was made. Pressed poly(tetrafluoroethylene) powders were used as perfect reflector standards in calculating Kubelka−Munk pseudoabsorbances. N_2 physisorption adsorption and desorption isotherms, BET surface areas, and BJH pore size distributions were recorded at the boiling point of liquid N_2 in a Micromeritics ASAP 2010 instrument with prior 8 h degassing at 120 °C. A Shimadzu GC-2010 gas chromatograph (GC) was used with a flame ionization detector (FID), a Thermo Scientific TR-1 column (30 m × 0.25 mm i.d. × 0.25 μm), He carrier at constant linear velocity of 60 cm/s, and a program of 3 min at 50 °C, 50 °C/min to 270 °C, 2 min hold. Products were identified by comparison to authentic standards and by gas chromatography/mass spectroscopy (GCMS) with a Hewlett-Packard HP 6890 series GC system equipped with a HP 5792 series mass-selective detector.

2.2. Synthesis of Mn Complexes. All reagents were used as received from Sigma-Aldrich unless otherwise noted. Although 1,4,7-trimethyl-1,4,7-triazacyclononane (tmtacn) can be obtained commercially (e.g., TCI America), a high-yield synthesis is given in the Supporting Information, modified from the literature.[19]

Mn-tmtacn dimer **1**, $[Mn_2(tmtacn)_2(\mu\text{-}O)_3](PF_6)_2\cdot H_2O$, was synthesized following literature protocol[19,20] from tmtacn (0.68 g, 4.0 mmol) in 8 mL of 2/1 EtOH/H_2O, $MnCl_2\cdot 4H_2O$ (0.8 g, 4.0 mmol), KPF_6 (1.1 g, 6.0 mmol), and 1/1 H_2O_2 (1.5 M)/NaOH (1.0 M). Large red crystals were obtained following crystallization from MeCN/EtOH and washing. Yield: 0.65 g (42%). MS (ESI^+, MeCN): m/z 645.17 ($[M - PF_6]^+$), 501.21 ($[M - 2PF_6]^+$). Elemental analysis: found (calcd $Mn_2C_{18}H_{44}N_6O_4P_2F_{12}$) C 26.9 (26.7), N 10.3 (10.4), Mn 13.0 (13.6).

For the purposes of empirical spectral comparison, known acetate-bridged Mn-tmtacn dimer **2b**, $[Mn_2(tmtacn)_2(\mu\text{-}O)(\mu\text{-}OOCCH_3)_2](PF_6)_2$, was synthesized from tmtacn (202.5 mg, 1.2 mmol), *p*-toluenesulfonic acid monohydrate (199.0 mg, 1.0 mmol) in 10.0 mL of MeCN, $Mn(OAc)_3\cdot 2H_2O$ (269.5 mg, 1.0 mmol), KPF_6 (234.3 mg, 1.3 mmol), CH_3COONa (205.1 mg, 2.5 mmol), and $NaHCO_3$ (84.7 mg, 1.0 mmol) following literature protocols.[19,20] A dark purple solid was obtained after washing and recrystallization from MeCN/EtOH. Yield: 207.2 mg, 0.236 mmol (47%). MS (ESI^+, MeCN): m/z 731.21 ($[M - PF_6]^+$), 586.25 ($[M - 2PF_6]^+$), 543.23 ($[M - CH_3CO - 2PF_6]^+$). Elemental analysis: found (calcd $Mn_2C_{22}H_{48}N_6O_5P_2F_{12}$) C 30.1 (30.2), N 9.4 (9.6), Mn 12.5 (12.5).

2.3. Solid Cocatalyst Synthesis. Mesoporous silica gel (Selecto Scientific, 32−63 μm particle size, BET surface area 500 m^2/g) was treated at 120 °C under dynamic vacuum for 12−15 h prior to grafting. 2-(Carbomethoxy)ethyltrimethoxysilane was used as obtained from Gelest, Inc. The dried support (1−2 g) was suspended in 50 mL of anhydrous pyridine under an inert atmosphere, and 0.2−4.0 mmol of 2-(carbomethoxy)ethyltrimethoxysilane was added per gram of SiO_2, heated to 125 °C, and heated at reflux with stirring for 18−24 h. The solids were filtered on a glass frit, washed with toluene (200 mL) and ether (50 mL), Soxhlet extracted for 24 h in benzene to remove ungrafted ester, and dried under a vacuum. The surface esters were subsequently heated at reflux in 1.0 M HCl for 18−24 h, Soxhlet extracted with water for 18−24 h, dried under a vacuum, and then stored in a desiccator until use.[21] Where applicable, support particles were separated by size after hand-grinding with mortar and pestle using USA Standard Testing Sieves. The final product is referred to simply as "cocatalyst".

2.4. Surface Structure by X-ray Absorption Spectroscopy and DFT. For X-ray absorption spectroscopy (XAS) of surface structures formed under reaction conditions, **1** (14−40 mg) was dissolved in 20 mL of MeCN, and then ∼250 mg of support (SiO_2 or solid cocatalyst with acid/Mn = 2−3, resulting in 0.5−1.4 wt % Mn) and 2.0 mL of H_2O or 30 wt % of H_2O_2 was added. The mixture was stirred at 25 °C for 3 h. The solids were then filtered on glass fiber filter paper and washed with 100−200 mL of MeCN and 50 mL of Et_2O. XANES and EXAFS data were collected on the DuPont−Northwestern−Dow Collaborative Access Team (DND-CAT) beamline at bending magnet station 5-BMD at the Advanced Photon Source, Argonne National Laboratory. This X-ray source provides a dedicated 7 GeV, 100 mA source over an energy range of 4.5−80 keV, controlled by a Si(111) monochromator and resolution of 10^{-4}. The monochromator was calibrated with Mn foil to the first inflection point of the edge, an energy of 6539.0 eV.[22] Known standards (MnO, MnO_2, Mn_2O_3) were brushed onto adhesive tape and analyzed in transmission mode by spectroscopy-grade ionization chambers.[23] Solid catalyst samples (25−30 mg) were vacuum-dried, finely ground, pressed into self-supporting wafers, and attached to a stainless steel rack with Kapton tape.[24] Sample fluorescence was acquired with a 13-element solid-state detector, which has proven to be a useful method for characterizing dimanganese and manganese-μ-oxo structures.[25] Data from each detector were normalized using a cubic polynomial and averaged in Athena. The atomic background was removed using a spline.[26] Edge energies are reported as the first inflection point along the edge. Fourier transforms were calculated over 2.3−9.0 $Å^{-1}$, isolating the region with a Hanning window function (dk = 1).

In EXAFS analysis, eq 1 was used for modeling and fitting. To develop EXAFS simulations from DFT or published single-crystal X-ray diffraction (XRD) structures, the coordination number, N_S, and half-path length, R_{as}, were fixed according to the model; the passive electron reduction factor, S_0^2, and the Debye−Waller factor or mean-squared displacement, σ_{as}^2, were set to 1 and 0.003, respectively. Only the threshold energy, E_0, was allowed to vary along the measured Mn K-edge jump to best align k. In all model fits, S_0^2 and the edge energy were varied independently. The Debye−Waller factor was varied for each element (O, Mn, N, and C). R_{as} was also varied for each element and, with the variation from the original model, set proportional to the effective distance from the Mn adsorbing atom.[24,27] The k-weights, k^1, k^2, and k^3, were fit simultaneously to reduce the impact of data analysis on the quality of the fit.[26] Theoretical scattering amplitude, $A_s(k)$, path degeneracy, N_s, and phases, $\varphi_{as}(k)$, were calculated by FEFF6 using the structure provided to ATOMS.[28] By applying a Hanning window function (dr = 0), structures were fit in R-space over the range 1.0−3.6 Å.

$$\chi(k) = \sum_s \frac{N_S S_0^2 A_s(k)}{kR_{as}^2} \exp(-2k^2\sigma_{as}^2) \sin(2kR_{as} + \phi_{as}(k)) \quad (1)$$

DFT calculations were performed using the Vienna Ab Initio Simulation Package.[29] A plane-wave basis set with a cutoff energy of 400 eV and ultrasoft Vanderbilt pseudopotentials[30] was employed. Calculations adopted the Perdew−Wang (PW-91) form of the generalized gradient approximation[31] exchange and correlation functional. The DFT calculated energies were subsequently adjusted by inclusion of dispersion forces per the method of Grimme.[48] The Bader analysis method developed by Henkelman and co-workers[32] was used for charge analysis. The Brillouin zone for the supported catalyst was sampled with a uniformly dense 2 × 2 × 1 k-point grid (Monkhorst pack),[33] and the Brillouin zone for the calculation of **1** was sampled with a single k-point at the gamma point. The structures' geometries were optimized within a convergence tolerance of 10^{-3} eV. A model for the β-cristobalite SiO_2(111) surface has been previously developed by Yang et al.,[34] with isolated silanols separated by 5 Å. In our work, a 3 × 3 unit cell was adopted, and two of the silanol groups were replaced by two propionic acid groups. Complex **1** was attached to the surface through one, two, or three carboxylic acid groups, forming **2a′**, **2b′**, and **2c′**, respectively. Related structures with cleaved Mn−O−Mn bonds were also modeled.

2.5. Cyclooctene Oxidation. *cis*-Cyclooctene (Sigma-Aldrich) was distilled over powdered NaOH through a Vigreux column under N_2, passed through an activated neutral alumina column, and stored under N_2.[35] All other chemicals were used as received from Sigma-Aldrich, unless otherwise noted.

Batch kinetic reactions were carried out in 100 mL round-bottom flasks with magnetic stirring. As an example for determining the effect of solid cocatalyst ratios, a desired amount of solid cocatalyst, HPLC-grade MeCN (44.4 mL), *o*-dichlorobenzene (2.0 mL) as internal standard, and **1** (5.4 mg, 6.8 μmol) were added to the reaction flask, and it was brought to thermal equilibrium in an aluminum block on a Thermoelectrics Unlimited, Inc. cold-plate stirrer.

In method A, 30 wt % aqueous H_2O_2 (often 2.6 mL) was added and stirred at the reaction temperature for 40 min to allow for catalyst assembly on the solid. Iodometric titration[36] was performed on aliquots of the reaction mixture at the beginning and end of this pretreatment period to quantify oxidant consumption prior to alkene introduction. Following pretreatment, *cis*-cyclooctene (often 1.0 mL) was added and stirred for a specified time (typically 5−6 h). This reaction mixture corresponds to a molar ratio of **1**:*cis*-cyclooctene:H_2O_2 ≈ 0.001:1.0:3.4. Aliquots of the reaction solution were removed periodically and filtered through Whatman GF/F syringe filters. A small amount of Ag powder was then added to the aliquots, which were subsequently analyzed by GC. The Ag decomposed residual H_2O_2, terminating possible background reactions prior to analysis, and, more importantly, prevented overoxidation of reaction products during GC analysis. In control reactions, the Ag powder was unreactive with the reaction products. The concentrations of *cis*-cyclooctanediol, *cis*-cyclooctene oxide, and residual *cis*-cyclooctene were monitored and their identities verified by GCMS and comparison to commercial standards. The mass balance (produced *cis*-cyclooctanediol + *cis*-cyclooctene oxide per *cis*-cyclooctene consumed) was between 90% and 105% for all reactions.

In method B, once the reactor containing cocatalyst, MeCN, *o*-dichlorobenzene, and **1** reached thermal equilibrium, *cis*-cyclooctene was added and stirred for 10 min. Substrate oxidation was then initiated by addition of 30 wt % aqueous H_2O_2. Product analysis was as for method A. Screening reactions with analysis only at reaction completion were carried out by scaling down by a factor of 20 and with near-simultaneous addition of all species in 3 mL conical vials with Teflon-lined caps.

Method C was carried out as in method B, except that 30 wt % aqueous H_2O_2 was added slowly by syringe pump (polypropylene or poly(tetrafluoroethylene) for all wetted parts) over a specified amount of time. For all method C runs, a total of 2.6 mL of 30 wt % H_2O_2 (mol ratio of **1**:*cis*-cyclooctene:H_2O_2 ≈ 0.001:1.0:3.4) was added. Product analysis was as for method A.

3. RESULTS AND DISCUSSION

3.1. Support Synthesis. We and others have described the synthesis and characterization of ester- and carboxylic acid-functionalized SiO_2.[17,21] Many routes are available to synthesize solid supports possessing such groups,[21,37] and most could likely be used here. Surface esters and carboxylic acids were confirmed by ^{13}C CP/MAS NMR spectroscopy (Figure S1).[21] Loadings and corresponding average surface densities of the ester and final carboxylic acid groups (Figure S2) were calculated from TGA mass loss relative to unfunctionalized supports and were found to range from 0.2 to 1.3 ester nm^{-2} SiO_2 (0.16−1.07 mmol of ester

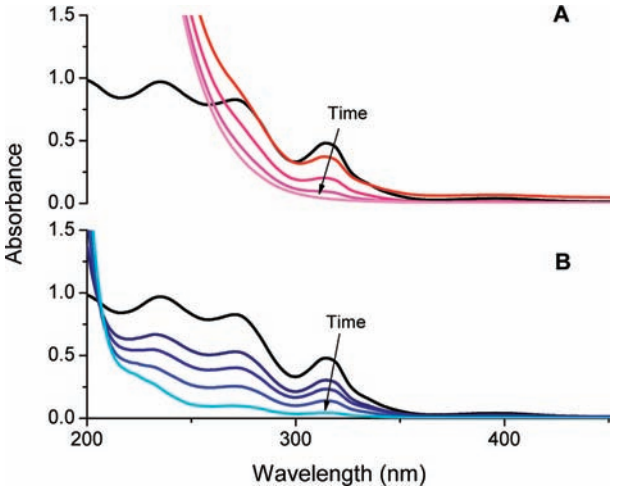

Figure 1. Solution UV−visible spectra of **1** (black) in (A) MeCN/H_2O_2 and (B) MeCN/H_2O in contact with the solid cocatalyst, demonstrating loss of solution species with time as they either (A) assemble to form **2′** or (B) physically adsorb unchanged on the cocatalyst surface over 120 min. Background absorption below 275 nm in panel A is due to H_2O_2. Conditions: 0 °C, 0.05 mM **1**, acid/Mn = 2, 0.05 M H_2O_2 with 0.19 M H_2O from 30 wt % H_2O_2(aq) or 0.27 M H_2O. Solution depletion is much more rapid at typical H_2O_2 concentrations, but clean spectra could not be so obtained.

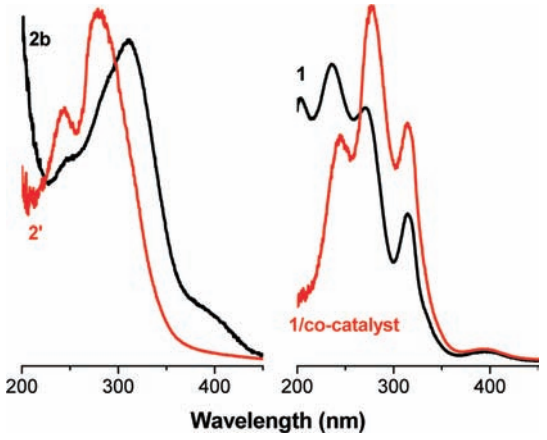

Figure 2. (Left) Normalized solution UV−visible spectrum of **2b** in MeCN and diffuse reflectance spectrum of **2′** via *in situ* heterogenization of **1** on solid cocatalyst from MeCN/H_2O_2. (Right) Normalized solution UV−visible spectra of **1** in MeCN, and diffuse reflectance spectrum of **1** physisorbed on the solid cocatalyst from MeCN/H_2O showing no change in structure.

(g SiO_2)$^{-1}$) or from 0.06 to 0.75 acid nm^{-2} SiO_2 (0.06−0.63 mmol of acid (g SiO_2)$^{-1}$), depending on the concentration of silane used in the initial grafting step. The acid treatment used to generate the free carboxylic acid also appeared to remove the more weakly bound silanes. Unless otherwise stated, all experiments in this study used solid cocatalyst possessing acid site density ranging from 0.51 to 0.75 acid nm^{-2} SiO_2 (0.41−0.63 mmol of acid (g SiO_2)$^{-1}$); our previous studies indicated that, for this method of cocatalyst synthesis, carboxylate loading had negligible effect on catalyst productivity within this range.[17] N_2 physisorption BET surface areas decreased from 576 m^2 g^{-1} for SiO_2 to 508 m^2 g^{-1} for the cocatalyst to 489 m^2 g^{-1} for the

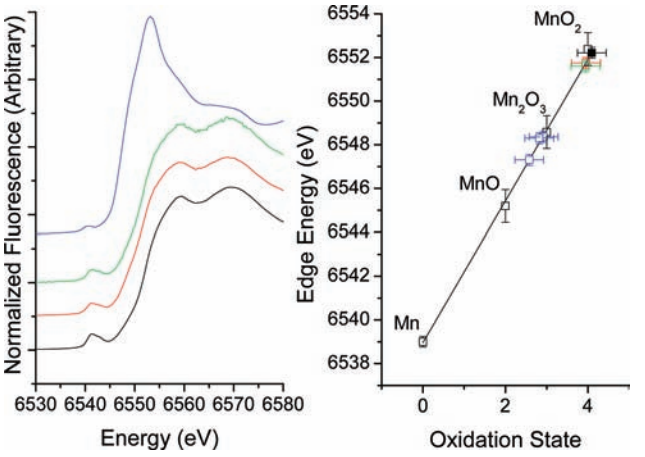

Figure 3. X-ray absorption near-edge spectra and their extrapolated edge energies indicating a change in metal oxidation state as the μ-oxo bridges of **1** (solid black) are replaced with μ-carboxylate bridges from the cocatalytic support upon formation of surface-bound complex **2′** (blue) from MeCN/H_2O_2 solutions. Three different catalyst preparations yield the same apparent surface structure. Physisorption of **1** on either SiO_2 (red) or the carboxylic acid-modified SiO_2 (green) from MeCN solutions with no H_2O_2 present produced no oxidation state changes. The experimentally determined edge energies of Mn standards (open black; Mn, MnO, Mn_2O_3, and MnO_2, as labeled) are given as reference.

Mn-containing catalyst. BJH desorption pore size distributions showed a corresponding decrease in the median pore diameter from 5.2 to 5.1 to 5.0 nm (see Supporting Information). These systematic and relatively minor changes are consistent with even dispersion of the grafted groups and Mn onto the SiO_2 surface, as opposed to grafting at the pore mouth or formation of large crystallites.

3.2. Assignment of the Supported Complex 2′. Transmission UV−visible (UV), DRUV, and XAS were used to characterize the supported and soluble Mn complexes and were compared to predictions from DFT. First, depletion of **1** from solution and concomitant adsorption of **1** onto supports is demonstrated by UV of MeCN solutions (with or without H_2O_2) of **1**, regardless of whether contacted with solid cocatalyst or with unfunctionalized SiO_2 (Figure 1). By qualitative comparison of DRUV (Figure 2) and XANES and the quantitative values of the extrapolated XANES edge energies (Figure 3), the $Mn^{IV,IV}$ complex **1** deposits on bare SiO_2 unchanged in structure or oxidation state. Complex **1** is likewise unchanged by adsorption on the solid cocatalyst in the absence of H_2O_2. In all cases, the observed Mn oxidation state is assigned as 4+ by comparison to MnO_2.

In contrast, when **1** is deposited on the solid cocatalyst from MeCN/H_2O_2 solutions, XANES and DRUV spectra show significant changes, indicating the formation of a new surface complex **2′**, which in principle could be any of three surface structures **2a′**, **2b′**, or **2c′** (Scheme 1) with one, two, or three bridging carboxylates, respectively. In addition to compound **2b** described in the Experimental Methods, solution complexes with one and three bridging carboxylates are known and have published single-crystal XRD structures.[4a,38] Throughout this article, the notation **2′** will be used when referring to the assembly of **1** on the solid cocatalyst in the presence of H_2O_2, without assigning a particular surface structure. Three distinct catalyst

Scheme 1. Coordination of 1 with Soluble Acids To Form Generic Structure 2, and Coordination with Solid Cocatalysts To Forms Generic Structure 2′ [a]

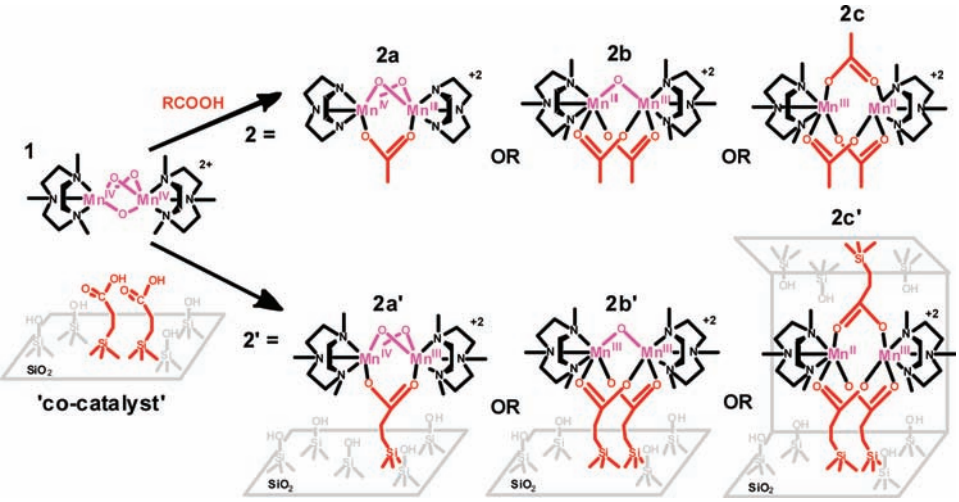

[a] The Mn complex may in actuality be coordinated to one, two, or conceivably three surface carboxylates, forming **2a′**, **2b′**, and **2c′**, respectively. Known soluble analogues for each of these structures (**2a**, **2b**, and **2c**) are also shown. Structures **1**, **2a′**, and **2b′** were modeled by DFT.

preparations (0.7 wt % Mn at acid/Mn = 2, 0.5 wt % Mn and 1.4 wt % Mn at acid/Mn = 3) using cocatalysts with an acid site density of 0.2−0.6 mmol g^{-1} show similar spectra and edge energies.

Optimal structures were calculated for **1**, **2a′**, **2b′**, and **2c′** (Scheme 1). The enthalpies of the formation reactions were calculated as

$$\mathbf{1} + {}^{1}/_{2}H_2O_2 + \text{supported carboxylate} = \mathbf{2a'} + H_2O + {}^{1}/_{2}O_2 \qquad -1.55\ \text{eV}$$

$$\mathbf{1} + H_2O_2 + 2(\text{supported carboxylate}) = \mathbf{2b'} + 2H_2O + O_2 \qquad -2.21\ \text{eV}$$

$$\mathbf{1} + {}^{3}/_{2}H_2O_2 + 3(\text{supported carboxylate}) = \mathbf{2c'} + 3H_2O + {}^{3}/_{2}O_2 \qquad -1.10\ \text{eV}$$

These results show that the formation of **2b′** is more favorable than the formation of **2a′** by 0.66 eV and of **2c′** by 1.1 eV. Surface structure **2b′** is also expected to have a more favorable entropy of formation. Adjacent dissociated monomers or alternate coordination geometries that share the same overall stoichiometry of **2b′** were much less stable in these simulations.

Replacement of each μ-oxo bridge in **1** with a bridging carboxylate decreases the average formal oxidation state of Mn by 0.5. Here, the reduction in the intensity of the XANES pre-edge feature and a shift of the edge to lower energy are both consistent with a decrease in the average formal oxidation state from 4+ to 3+, as calibrated by spectra of MnO_2, Mn_2O_3, and MnO. This corresponds to a change from $Mn^{IV,IV}$ complex **1** to $Mn^{III,III}$ surface complex **2b′** with two bridging carboxylates (Figure 3). While a mixture of **2a′** and **2c′** is also consistent with the observed average oxidation state, triply bridged $Mn^{III,II}$ structure **2c′** would require high-concavity regions on the SiO_2 particle surface to form and would have a less-favorable enthalpy of formation, and the low formal Mn oxidation state of 2+ is unlikely to be stable under experimental conditions. Thus, the observed average oxidation state is considered to be most consistent with $Mn^{III,III}$ **2b′** as the dominant surface species.

Bader charge analysis of the modeled surface species shows the calculated oxidation state of Mn in **1** shifting from +3.20 to +3.18 for **2a′**, to +3.03 for **2b′**, and to +2.48 for **2c′**. This is compared to the calculated partial charges on Mn in bulk MnO_2 (+3.88), Mn_2O_3 (+3.44), and MnO (+2.68).

Although this analysis does not match quantitatively with formal oxidation states of the complexes inferred from XANES due to varying levels of covalency in the complexes, it confirms that the observed reduction upon attachment is most consistent with the formation of surface species **2b′**.

Beyond comparison of oxidation state, the structure of **2′** is also assigned as **2b′** on the basis of a qualitative match of the DRUV experimental spectrum of **2′** with the UV spectrum of **2b** in MeCN (see Experimental Methods). The slightly higher peak energy for **2′** vs **2b** is attributed to the low dielectric air environment for **2′**; charge separation in the excited state is less favorable in low dielectric environments.[39]

Various models were fit to experimental EXAFS data of the surface species. None of the surface species were adequately fit with bulk MnO_2 or Mn_2O_3. However, even with no adjustment, the simulated *k*-space spectrum of **1** derived from the DFT model overlays well with the experimental *k*-space spectrum of **1** deposited on SiO_2 or on cocatalyst in the absence of H_2O_2 (Figure S4). Using the DFT model as a starting point, Table 1 and Figure 4 show that the bond distances from the optimized EXAFS structure of **1** physisorbed on SiO_2 differ only minimally from either the DFT or the XRD structure,[4a] indicating that **1** adsorbs as an intact dication under these conditions.

DFT models show Mn−Mn bond lengths systematically increasing from **1** to **2a′** to **2b′**. Consistent with the expected reduced symmetry of **2a′** and **2b′**, these structures show a range of Mn−N and Mn−O distances all larger than those of **1**. The calculated bond lengths for **2b′** agree well with those derived from published XRD structures of **2b**.[40] No XRD structure is available for a direct molecular analogue of **2a′**; instead the bond

Table 1. EXAFS Fit Parameters at the Mn K-Edge for Supported Complexes 2′ and 1: Calculated, Fit, or Observed Bond Distances (Å)[a]

bond	DFT	EXAFS	XRD[b]	EXAFS-DFT	σ_f
			2b′ (R_f = 0.012)		
μO	1.93	1.96(3)	2.054(4)		
cO	2.19	2.22(3)	2.132(6)	0.03	0.005(6)
cO	2.24	2.27(3)	2.201(6)		
N1	2.34	2.6(2)	2.286(7)		
N2	2.44	2.7(2)	2.329(7)	0.2	0.000(1)
N3	2.69	2.9(3)	2.343(8)		
Mn−Mn	3.09	2.9(1)	3.353(3)	−0.1	0.010(6)
C (avg)	3.16	3.6(1.2)	3.11(3)	0.4	0.02(1)
			2a′ (R_f = 0.009)		
μO	1.96	1.7(2)	1.809(3)		
μO	1.97	1.8(2)	1.816(3)	−0.2	0.006(4)
cO	2.25	2.0(2)	2.079(5)		
N1	2.43	2.6(2)	2.105(3)		
N2	2.43	2.6(2)	2.108(5)	0.2	0.000(1)
N3	2.53	2.8(2)	2.136(6)		
Mn−Mn	2.66	2.45(20)	2.588(3)	−0.2	0.009(9)
C (avg)	3.19	3.3(4)	2.97(2)	0.1	0.04(9)
			1 (R_f = 0.009)		
μO	1.82	1.81(3)	1.820(6)		
μO	1.82	1.81(3)	1.820(6)	0.01	0.007(2)
μO	1.83	1.82(3)	1.833(7)		
N1	2.11	2.08(6)	2.106(7)		
N2	2.11	2.08(6)	2.106(7)	0.02	0.000(1)
N3	2.11	2.09(6)	2.109(9)		
Mn−Mn	2.30	2.27(4)	2.297(3)	−0.03	0.001(3)
C (avg)	2.91	2.8(1)	2.91(4)	−0.1	0.005(6)

[a] Overall goodness of fit R_f, average atomic distances, and Debye−Waller factors, σ_f, are given for the optimized structures derived from experimental EXAFS data. Standard error is given in parentheses. Bond distances as determined by DFT, and published XRD are also provided. Bridging μ-oxo atoms (μO) are distinguished from carboxylate O atoms (cO). [b] For **2b′**, XRD data are from ref 40. For **2a′**, the mixed-valent Mn^{III}−Mn^{IV} coordination complex crystal structure was determined with 1,4,7-triazacyclononane ligands, not tmtacn; data are from ref 38. For **1**, XRD data are from ref 4a.

lengths for the triazacyclononane analogue are given in Table 1.[38a] This and structures with constrained, bridged triazacyclonane ligands[38b] have much shorter Mn−O and Mn−N distances than those calculated for **2a′** by DFT. In general, the expanded bond lengths are expected from higher steric hindrance and from π-electron donation from the carboxylate. The simulated spectra of **2a′** or **2b′** derived from DFT models (Figure S4) were used as starting points for fitting the EXAFS of **2′**. After uniformly increasing or decreasing bond distances for a given element shell, both starting structures produced an adequate fit based on overall R_f (Figure 4, Table 1) and given the signal-to-noise for these low-loaded Mn catalysts. Importantly, structure **2b′** required only small changes in the critical Mn−O and Mn−Mn distances relative to those calculated by DFT: a 0.03 Å increase and a 0.19 Å decrease, respectively. Both changes were within the standard error of the experimental EXAFS structure.

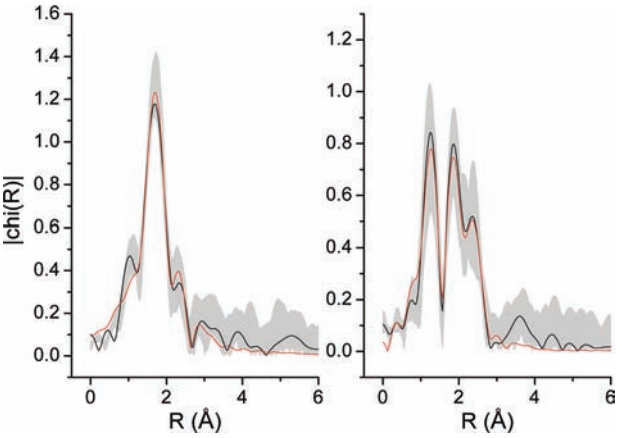

Figure 4. Transformed Mn K-edge EXAFS giving the magnitudes of k^2-weighted Fourier-transformed spectra: (left) **1** contacted with cocatalyst in the presence of H_2O_2; (right) **1** on bare SiO_2. Gray region represents the range of all experimental spectra collected from 13 fluorescence detectors, averaged over all scans. Black curves are the averaged experimental spectra of all detectors and scans. Overlaid in red are the resulting fits starting from **2b′** (left) and **1** (right). Corresponding structural parameters are given in Table 1.

The optimized Mn−O distances also agree well with a published XRD structure.[40] Regardless of the model, Mn−N and Mn−C bonds required larger increases in bond lengths from those of the DFT structure for an adequate fit, but larger standard error was also associated with these more distant and low mass scatterers. It is also likely that the steric effect of the surface displaces the tmtacn ligand somewhat. In contrast, fitting the experimental spectrum starting from structure **2a′** could not be done with high precision for Mn−O and Mn−Mn, and resulted in unreasonably short Mn−O distances similar to those of **1** or the constrained complexes for which XRD structures are given. Combined with the observed 3+ average oxidation state, the $Mn^{III,III}$ structure **2b′** is most consistent with all observed spectra of the catalytic surface species.

3.3. Catalytic Behavior. A series of screening reactions were carried out at 0 °C in a sealed batch reactor to investigate the effect of the cocatalyst loading, expressed here as the carboxylic acid to Mn ratio (acid/Mn), on the total cyclooctene oxidation productivity after 5 h (Table 2). High oxidation productivities were achieved at acid/Mn ≥ 1, consistent with doubly coordinated Mn dimer **2b′** being a catalytically relevant species. The empirical advantage of the surface-displayed carboxylic acids was also seen, with 1 equiv of surface carboxylic acid giving productivities only matched by 1000 equiv of soluble valeric acid, a quantity of cocatalyst more than the total amount of epoxide and *cis*-diol products. From an applications standpoint, eliminating soluble cocatalysts also simplifies downstream separation and purification in preparative reactions. As some of us previously reported, **2′** demonstrates high productivity for a number of diverse alkenes, with decreased productivity only for particularly hindered or electron-deficient species.[17] Neither control reaction (SiO_2 + **1** or SiO_2 + **1** + valeric acid) produced significant quantities of epoxide or *cis*-diol, eliminating the possibility of catalysis by leached carboxylic acid groups or a role for bare SiO_2 in activating **1**. Filtrates of the solution in contact with the solids were catalytically inactive, even upon addition of fresh portions of solid cocatalyst and H_2O_2, ruling out catalytic activity of soluble species leached from the surface of the active catalyst (Figure S5).

Table 2. Cyclooctene Oxidation with 1 and Various Cocatalysts under Equivalent Conditions[a]

catalyst	acid/Mn	t (h)	T (°C)	ox. addn.	TOF_{max} (h^{-1})	t_{200} (min)	total TON	diol selectivity (%)
1	0	5	0	B			15	54
1 + SiO_2	0	5	0	B			<5	
2′	1	5	0	B			140	37
2′	2	6	0	B	135	100	465	45
2′	2	6	0	A	300	40	480	45
2′	2	6	0	C	140	130−180[b]	465	40
2′	2	3	25	A	600	20	530	45
2′	2	10	−10	A	100	120	510	50
2′	10	5	0	B			680	42
2′	10	5	0	A			715	36
1 + valeric acid	1	5	0	B			15	63
1 + valeric acid + SiO_2	10	5	0	B			5	50
1 + Valeric acid	10	5	0	B			65	75
1 + valeric acid	1000	5	0	B			150	64

[a] Batch reactor, 5 h reaction, 0 °C, MeCN, 0.13 mM 1, 0.15 M *cis*-cyclooctene, 0.51 M H_2O_2 (130 μL of 30 wt % H_2O_2), TON ≈ 1000 for 100% yield. [b] Semibatch oxidant addition at 0.7 or 1.4 mL of H_2O_2 h^{-1}.

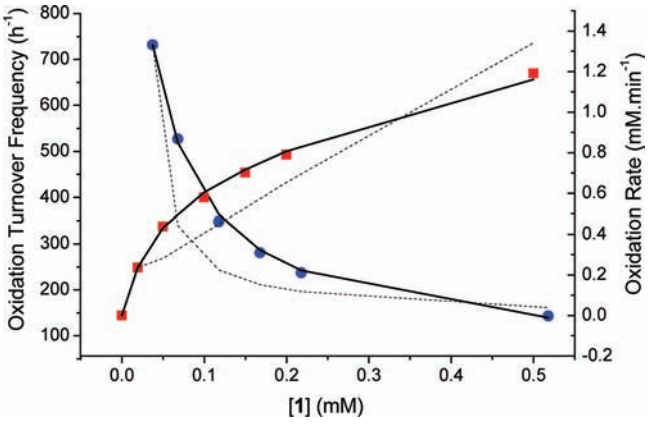

Figure 5. Total cyclooctene oxidation initial rate (□) and initial turnover frequency (○) plotted against catalyst concentration for a constant amount of solid cocatalytic support equivalent to 0.56 mM. Rates are modeled assuming adsorption and activation of **1** on one carboxylate (dashed line) or adsorption and activation of **1** on two carboxylates (solid line). Model details are provided in the Supporting Information. Conditions: 0 °C, 0.56 M H_2O_2, and 0.17 M *cis*-cyclooctene.

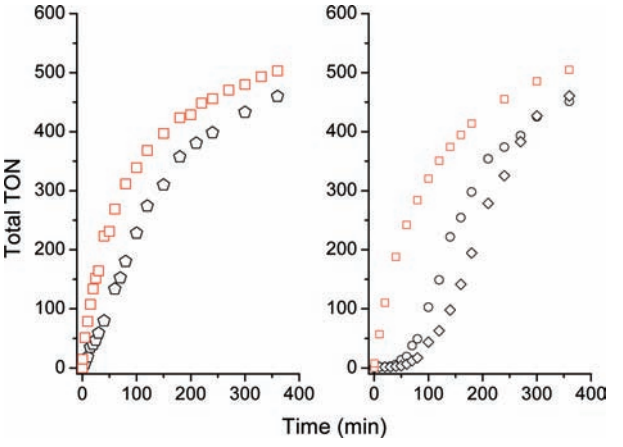

Figure 6. Total turnovers for *cis*-cyclooctene oxidation by H_2O_2 and **2′** (acid/Mn = 2) at 0 °C. (Left) H_2O_2 pretreatment, method A (□), and without H_2O_2 pretreatment, method B (⬠). (Right) Slow H_2O_2 addition, method C, at 1.4 mL of H_2O_2 h^{-1} (○) and 0.7 mL of H_2O_2 h^{-1} (◇) compared to H_2O_2 pretreatment method A (□). Conditions: 0.15 mM **1**, 0.56 M H_2O_2, and 0.17 M *cis*-cyclooctene.

Initial cyclooctene oxidation rates were determined by method A with varying initial concentration of **1** while holding constant the amount of solid cocatalyst (Figure 5). At low amounts of added **1** (large acid/Mn), most of the Mn acts as an active surface species, giving a high apparent initial turnover frequency (TOF_0, (moles epoxide + moles *cis*-diol) per mole **1** per time, extrapolated to zero time). With increasing amounts of **1** (smaller acid/Mn), the available surface sites become progressively saturated, giving asymptotically higher total rates but lower TOF_0 because an increasing number of Mn centers may not be coordinated to carboxylates and thus not participating in the reaction. With the assumption that each coordinated surface species has the same intrinsic reactivity, the rates follow a Langmuir model requiring two adsorption sites (surface carboxylic acids) for each complex **1** (Figure 5, for raw data and discussion see Figure S6); a one-site model was unable to capture the curvature of the data. This fit is consistent with the active species being structure **2b′**, which requires two surface acid groups as adsorption and activation sites for each **1**. Practically speaking, TOF_0 was deemed to be adequate at acid/Mn = 2, avoiding excessive amounts of cocatalyst in most investigations.

3.4. Oxidation Kinetics. *3.4.1. Oxidation Induction Period and H_2O_2 Addition Rate.* *cis*-Cyclooctanediol and *cis*-cyclooctene oxide production was monitored as a function of time for three different methods of H_2O_2 addition, as described in the Experimental Methods. Batch H_2O_2 addition method B and slow H_2O_2 addition method C (Figure 6) each involved addition of substrate before oxidant and exhibited induction periods prior to onset of substrate oxidation. This induction period is well known in studies with the homogeneous catalyst and is consistent with the conversion of **1** into a new species that is part of the catalytic cycle or a direct precursor. Complex **2b**, with replacement of two bridging O with bridging carboxylate ligands, has particularly been proposed as the active species for **1** + acetate.[14] Batch H_2O_2

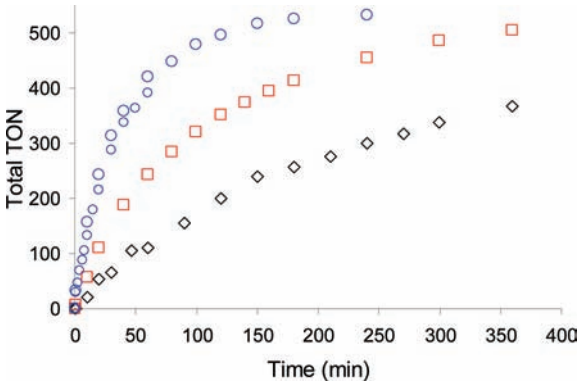

Figure 7. Total turnovers in *cis*-cyclooctene oxidation by H_2O_2 and **2′** (acid/Mn = 2) at −10 (◇), 0 (□), and 25 °C (○) with H_2O_2 pretreatment (method A). Initial rates increase with increasing temperature, while total productivity is similar for all temperatures with sufficiently long reaction times. Conditions: 0.15 mM **1**, 0.56 M H_2O_2, and 0.17 M *cis*-cyclooctene.

addition method A (Figure 6), with its 40 min H_2O_2 pretreatment of the mixture of **1** and solid cocatalyst prior to substrate addition, showed product formation within 30 s of alkene addition. This is consistent with formation of a catalytically relevant surface species **2′** upon reaction with H_2O_2 before the alkene is added. In homogeneous systems, it has likewise been shown that the induction period could be minimized by directly using previously synthesized **2b** or by forming the carboxylate-bridged complex *in situ* during H_2O_2 pretreatment of **1** in the presence of carboxylic acid.[14]

Controlling H_2O_2 decomposition (catalase activity) by **1** and related Mn species is a critical determinant in choosing the acid cocatalyst and a potential limitation to industrial application in synthetic chemistry.[7b,13,14] In the majority of published homogeneous studies where the goal was chemical synthesis rather than bleaching, temperatures of ≤0 °C and slow H_2O_2 addition were utilized to boost yields by limiting radical reactions and unproductive H_2O_2 decomposition. This implicitly assumes that H_2O_2 decomposition (or the formation of a species catalytically active for H_2O_2 decomposition) is higher order in H_2O_2 and has a higher activation energy (E_a) than productive oxidation. Therefore, it is important to note that, when reaction and analysis conditions were identical, the total productivity of heterogenized **2′** after 6 h was largely independent of the method of oxidant addition (method A, B, or C, Figure 6). Que and co-workers noted that proper choice of soluble acid cocatalyst enabled batch addition of H_2O_2 with no loss in productivity in a related Fe system,[41] but no such tolerance has yet been exhibited for these Mn complexes. For subsequent work, we therefore utilized H_2O_2 method A (H_2O_2 pretreatment), which simplified the kinetic analysis by removing effects of the rate of formation of structure **2′** and allowed substrate oxidation rates to not be limited by the rate of H_2O_2 addition. Tolerance to higher initial H_2O_2 concentrations in batch addition of H_2O_2 also conferred significant practical advantages: by method A, 200 turnovers (total TON, (moles of epoxide + moles of *cis*-diol) per mole **1**) were reached 40 min after substrate addition at 0 °C, but by method B, TON = 200 required 2−3 h at 0 °C for typical H_2O_2 addition rates (Table 2). Maximum TOFs (Table 2) were not substantially affected by method of oxidant addition, but they occurred at earlier times for batch addition of H_2O_2.

3.4.2. Temperature Effects and Overall Yields. Product evolution for the H_2O_2-pretreated catalyst (method A) **2′** was analyzed at 25, 0, and −10 °C. Progressively lower temperatures reduced initial turnover rates of oxidation, in accordance with classical Arrhenius kinetics, from approximately 600 to 300 to 100 h^{-1} (Table 2). At 25 °C, the highest possible TOF was calculated to be ∼0.4 s^{-1} (over the first 30 s of reaction), which is of the same order of magnitude expected for internal diffusion rates. Therefore, the original solid cocatalyst was dry-sieved, and product evolution was monitored for solid cocatalyst particles >180 μm and for those <65 μm in diameter. No pronounced effect was observed for initial rates of product formation, but the larger particle size decreased ultimate productivity by 25% relative to the smaller particles (Figure S7), suggesting that the larger particle sizes are more prone to deactivation.

Using only the smaller particles for the 25 °C reaction, it was seen that total productivities are also largely independent of reaction temperature over this solid catalyst (Figure 7), as they were similarly insensitive to oxidant addition method. The practical effect is that this catalyst can be utilized at 25 °C with no reduction in total productivity, but with much lower processing time. By method A, TON = 500 was reached at 120, 360, and 800 min at 25, 0, and −10 °C, respectively.

The $2e^-$ reduction of **1** into soluble bis(μ-carboxylato) complex **2b** occurs over 0.5−1.0 h, accompanied by stoichiometric oxidation of H_2O_2 to O_2.[4c,5,14,37b] H_2O_2 is consumed in forming the epoxide and diol products, but also in undesired decomposition to O_2 and H_2O. H_2O_2 concentrations were thus monitored during pretreatment (no substrate) and during the oxidation reaction for the supported catalyst at −10, 0, and 25 °C (Figure S3). During the 40 min pretreatment of method A, ∼400 equiv (per added **1**) of H_2O_2 is decomposed at 0 °C, ∼70 equiv at −10 °C, and ∼1500 equiv at 25 °C. Excluding the pretreatment period, H_2O_2 utilization $((mol_{epoxide} + mol_{cis\text{-}diol})/(mol_{H_2O_2})_0)$ was 32% at TON ≈ 500 at a reaction temperature of 25 °C, but <15% for the longer times required to reach similar productivity for 0 and −10 °C operation. The substantial consumption of H_2O_2 in the absence of alkene at 25 °C may be catalyzed by unobserved minority species like MnO_2. Although not a goal of this report, H_2O_2 decomposition in this period can presumably be minimized by optimizing pretreatment conditions, as has been accomplished for homogeneous catalysts.[14]

Under the conditions employed in this study, heterogenized catalyst **2′** reached a maximal productivity of TON = 715 with acid/Mn = 10 (Table 2). This productivity is similar to data reported in the open literature using soluble cocatalysts; however, varying conditions make direct comparisons difficult (Table 3).[13,14] It is also important to note that the vast majority of the optimized homogeneous catalyst formulations utilized strongly reducing (i.e., oxalic acid) or electron-withdrawing (i.e., trichloroacetic acid) cocatalysts in unison with subambient temperatures and slow oxidant addition rates, which mandate longer reaction times than our conditions. Moving to more electron-withdrawing surface-grafted acids may allow further increases in catalyst rate and productivity in this system.

3.4.3. Initial Rates and Rate Orders. Additional experiments were carried out in the oxidation of *cis*-cyclooctene at 0 °C with **2′** and aqueous H_2O_2 to determine apparent reaction orders of the various species (see Supporting Information for detailed experimental procedures). The effects on initial rates of cyclooctene conversion are compiled in Table 4 (raw data in Table S1 and Figure S6). Epoxide and *cis*-diol products were

Table 3. Optimized Soluble Acid Cocatalysts for 1 in the Oxidation of *cis*-Cyclooctene[a]

cocatalyst	acid/Mn	TON (yield, diol %)	ref
oxalate	3	410 (52, 0)	13d
oxalic acid[b]	1	740 (94, 24)	14b
CCl_3CO_2H	1	685 (91, 64)	13e
CCl_3CO_2H	25	730 (96, 45)	13e
salicylic acid	1	755 (82, 8)	13e
2,6-Cl_2PhCO_2H	3	600 (67, 88)	13e
SiO_2-carboxylate[c]	10	715 (71, 36)	this

[a] Unless otherwise given, conditions are 0 °C, slow addition of H_2O_2 over 6−7 h. [b] 25 °C. [c] 0°, single addition of H_2O_2, 5 h.

Table 4. Apparent Reaction Order of Tested Species[a]

component	apparent order
H_2O_2	1.00
cis-cyclooctene	0.18
H_2O	−0.13
epoxide	−0.05
cis-diol	−0.05

[a] See Supporting Information for reaction conditions, and Figure S4 and Table S1 for raw data.

found to minimally impact initial rates, indicating neither strong product inhibition nor competitive overoxidation. Deliberate addition of *trans*-cyclooctane diol, even though it is not formed under these conditions, also had a negligible impact on initial rates. The catalyst is first order in H_2O_2 concentration, but H_2O, which is necessarily produced during reaction, is only weakly inhibitory. The cyclooctene substrate is only weakly positive order.

Taken together, these results are consistent with a mechanism where the cyclooctene oxidation rate is limited by H_2O_2 activation. Rate-limiting formation of a dicarboxylate-bridged, dinuclear $Mn^{III}(OOH)Mn^{III}(OH)$ species has been identified as a critical intermediate step in alkene oxidation with soluble **1**.[14,15] This species forms by equilibrated coordination of H_2O, followed by rate-limiting formation of the Mn hydroperoxide. Unlike in solution, the equilibrium for H_2O coordination on the supported catalyst appears to favor products at all tested H_2O concentrations. This saturation behavior is responsible for the near-zero rate order for H_2O. Our DFT calculations showed that H_2O coordination to form a dicarboxylate-bridged, dinuclear $Mn^{III}(OH)Mn^{III}(OH)$ species from **2b′** is moderately more favorable by 0.05 eV. Higher order H_2O_2 decomposition reactions do not appear to impact oxidation rates, consistent with the observation of similar yields regardless of H_2O_2 concentration; all reactions that limit productivity are of the same apparent first order. The absence of a significant dependence on cyclooctene concentration is also consistent with our previous observation of high and similar turnovers at 3 h for a variety of alkene substrates —only particularly bulky and/or electron-deficient reactants showed notably decreased productivity, implying a shift in the rate-limiting step.[17]

Although *cis*- and *trans*-diol and H_2O were shown to only weakly affect the initial oxidation rate, increased amounts of these components decreased overall cyclooctene conversion at extended time (Figure S8), suggesting that accumulation of these species contributed to a slow deactivation of the active site. These limitations are likewise consistent with ultimate productivity being independent of H_2O_2 addition method or reaction temperature. Isolation, washing, and reuse of the catalyst or simple readdition of H_2O_2 after moderate conversion (50−70%) resulted in few additional turnovers, indicating that catalyst or cocatalyst stability is the primary limiting factor under these conditions.

Following the observation of a first-order dependence on H_2O_2, initial rate constants were calculated for the formation of oxidation products (epoxide and *cis*-diol) and the consumption of H_2O_2 (Table 5). While the narrow temperature range places large uncertainty on the calculations, the apparent activation energy (E_a) for oxidation product formation is 38 ± 6 kJ mol^{-1}, which falls within the range of activation energies reported for Mn-based H_2O_2 decomposition catalysts.[44] High rates impose large uncertainty, but the E_a for H_2O_2 decomposition is 30 ± 10 kJ/mol. The similar E_a for the two reactions is consistent with a common rate-limiting step of H_2O_2 activation, and in contrast with analogous homogeneous catalysts, this dictates that productivities are not limited by H_2O_2 consumption, even at 25 °C.

3.4.4. Epoxide:Diol Selectivity. Compared to epoxidation, relatively fewer catalysts are proficient at dihydroxylation, and fewer still are solid dihydroxylation catalysts.[42] *cis*-Diol selectivity was thus evaluated as a function of conversion for the conditions described above. Based on the ratio of initial rates, *cis*-diol selectivity was 30−40%, with no systematic changes with temperature (Table 5). Integrated selectivity reported at reaction completion was ∼45%, again relatively independent of temperature. Initial selectivities slightly underreport *cis*-diol content due to strong *cis*-diol adsorption on the SiO_2 carrier and nonlinear GC response at <5% yield. Above these minimum conversion levels, and for all temperatures investigated, differential selectivity (defined as selectivity between two consecutive time points) was constant at 40−50% (Figure S9), albeit with substantial scatter. The selectivity is not seen to change systematically with concentration of H_2O_2 or H_2O, the latter either added at the reaction outset or generated with increasing conversion. This insensitivity to reaction conditions is consistent with both epoxide and *cis*-diol products being formed from the same intermediate, and that product formation follows the rate-limiting step. Likewise, the *cis*-diol selectivity of homogeneous catalyst **2** was hypothesized to be dependent on the steric bulk of the associated carboxylate ligands, rather than on changes in the speciation of the active site.[7b,13,14] We hypothesize that selectivity can be controlled on surfaces by changing the nature of the solid cocatalyst or by altering the local surface microenvironment, which is currently under investigation.[45]

3.4.5. Side Reactions. The lack of *trans*-diol formation during typical oxidation conditions is evidence against free radical oxidation, which is expected to produce equivalent amounts of *cis*- and *trans*-diol. The reaction of epoxide with **2′** under conditions equivalent to cyclooctene oxidation also produces no *trans*-diol, further demonstrating the absence of significant acid-catalyzed ring-opening of the epoxide products. Minimal overoxidation of the *cis*-diol product is observed by GC-MS, primarily to α-hydroxy ketones, as typically reported, especially at high conversions.[13d,43] These products typically account for <10% of the total products, and it is difficult to ascertain whether oxidation occurs during catalysis or during GC workup, as we have observed

Table 5. Calculated Initial Rate Constants

T (°C)	$k_{ox,0}$ ($\times 10^5$ s^{-1})	$k_{epox,0}$ ($\times 10^5$ s^{-1})	$k_{diol,0}$ ($\times 10^5$ s^{-1})	initial diol selectivity (%)	$k_{H_2O_2,0}$ ($\times 10^5$ s^{-1})	initial H_2O_2 utilization (%)
25	5.6 ± 1.5	4.7 ± 1.8	2.2 ± 0.4	40 ± 10	45 ± 19	22 ± 5
0	2.7 ± 0.8	2.0 ± 0.4	0.6 ± 0.2	30 ± 10	19 ± 4	17 ± 3
−10	0.8 ± 0.1	0.5 ± 0.1	0.3 ± 0.05	40 ± 10	11 ± 2	9 ± 2
E_a	38 ± 6 kJ mol^{-1}				30 ± 10 kJ mol^{-1}	

transformation of standard *cis*-diol solutions containing trace H_2O_2 to overoxidation products upon high-temperature GC injection. For the purposes of this study, the overoxidation products observed were included in the *cis*-diol totals.

4. CONCLUSIONS

Throughout this article, parallels have been demonstrated between supported **2′** and soluble catalyst **2**. Therefore, the improved utility of the heterogenized catalyst can be understood in the context of the established mechanism of the homogeneous catalyst. First, given that the proposed active oxidant is a dicarboxylate-bridged, dinuclear $Mn^{III}(OOH)Mn^{III}(OH)$ species, the surface chelate effect will enhance coordination of carboxylates at low total concentrations, the hydrophilicity of the surface will encourage coordination of H_2O, and the SiO_2 surface may participate in H^+ transfer essential for coordinating and activating H_2O_2.[46] Stabilizing this active oxidant is proposed to account for increased rates, increases in productivity by slowing the formation of deactivated structures, and the relatively constant *cis*-diol selectivities regardless of carboxylate loading. In a key deviation from the homogeneous catalyst, similar total productivities are achieved at temperatures up to 25 °C, with H_2O_2 utilization at 25 °C at least as good as that at 0 °C. While catalase activity (H_2O_2 decomposition) is significant, it does not increase in rate with temperature any faster than for substrate oxidation, and under these conditions it never appears to be a limiting factor in overall productivity. In general, these mechanistic conclusions are expected to be a function of surface structure (oxide support, other chemisorbed groups, surface OH density, and pK_a), which is under investigation.

In conclusion, we have presented the synthesis and characterization of an efficient and active oxidation catalyst from the combination of Mn dimer **1** with carboxylates grafted on SiO_2 that function as both cocatalyst and support, allowing for assembly under reaction conditions. UV−visible and X-ray absorption near edge spectroscopy, extended X-ray absorption fine structure fitted to DFT models, observed dependence of rates on the acid/Mn ratios, and a rate law analogous to solution behavior all indicate the formation of an active catalyst precursor or resting state similar to **2b′** with two bridging carboxylates tethered to the surface. From an implementation point of view, these solid cocatalysts can be used exactly analogous to a soluble carboxylic acid cocatalyst but with total productivity, rates, and *cis*-diol selectivity that are high at low equivalents of carboxylic acid. Additional advantages of the heterogenized system are higher rates and insensitivity to typical parameters such as rate of H_2O_2 addition, temperature, and H_2O concentration. Empirically, this means that catalyst productivity can be boosted substantially: TON = 200 achieved in 20 min with batch addition of H_2O_2 at 25 °C as compared to 2−3 h for typical slow rates of H_2O_2 addition at 0 °C.

Given the broad scope of reactions catalyzed by **1** and other related non-heme complexes activated by carboxylic acids,[47] this one-pot synthetic and catalytic strategy may be useful for a number of reactions and catalyst/cocatalyst systems and is being tested as such. In comparison to typical soluble cocatalysts, this method of catalyst synthesis introduces new areas of reactivity control via modifications to the cocatalytic support. This promises to allow optimization of productivity and selectivity in ways not possible for traditional homogeneous catalysts.

■ ASSOCIATED CONTENT

Supporting Information. Detailed synthetic protocols for ligand and complex synthesis, support functionalization and characterization including ^{13}C CP/MAS solid-state NMR, and a comprehensive experimental description for cyclooctene oxidation and rate order determination, including detailed experimental results. This material is available free of charge via the Internet at http://pubs.acs.org.

■ AUTHOR INFORMATION

Corresponding Author
j-notestein@northwestern.edu

■ ACKNOWLEDGMENT

The authors thank The Dow Chemical Company and The Dow Methane Challenge, the Camille and Henry Dreyfus New Faculty Awards Program, a 3M Non-Tenured Faculty Grant, and Northwestern University for financial support. Portions of this work were performed at the DuPont-Northwestern-Dow Collaborative Access Team (DND-CAT) located at Sector 5 of the Advanced Photon Source (APS). DND-CAT is supported by E.I. DuPont de Nemours & Co., The Dow Chemical Company, and Northwestern University. Use of the APS, an Office of Science User Facility operated for the U.S. Department of Energy (DOE) Office of Science by Argonne National Laboratory, was supported by the U.S. DOE under Contract No. DE-AC02-06CH11357.

■ REFERENCES

(1) (a) Sheldon, R. A.; Kochi, J. K. *Metal Catalyzed Oxidations of Organic Compounds*; Academic Press: New York, 1981. (b) McGarrigle, E. M.; Gilheany, D. G. *Chem. Rev.* **2005**, *105*, 1563–1602. (c) Mandelli, D.; Voitiski, K. B.; Schuchardt, U.; Shul'pin, G. B. *Chem. Nat. Compd.* **2002**, *38*, 243–245.(d) Brinksma, J.; de Boer, J. W.; Hage, R.; Feringa, B. L. In *Modern Oxidation Methods*; Bäckvall, J.-E.; Ed.; Wiley-VCH: Weinheim, Germany, 2004; pp 295−326. (e) Kolb, H. C.; Van Nieuwenhze, M. S.; Sharpless, K. B. *Chem. Rev.* **1994**, *94*, 2483–2547.

(2) (a) Thomas, J. M.; Lewis, D. W. *Angew. Chem., Int. Ed.* **2005**, *44*, 6456–6482. (b) Sheldon, R. A. *J. Mol. Catal.* **1980**, *7*, 107–126. (c) Wong, O. A.; Shi, Y. *Chem. Rev.* **2008**, *108*, 3958–3987.

(3) Examples of recent literature reports: (a) Li, R.; Huang, F.; Jiang, X.; Liu, M.; Song, Y.; Liu, H.; Zhang, J. *J. Coord. Chem.* **2010**, *63*, 1611–1618. (b) Saikia, L.; Srinivas, D. *Catal. Today* **2009**, *141*, 66–71. (c) Serrano, D. P.; Aguado, J.; Vargas, C. *Appl. Catal., A* **2008**, *335*, 172–179. (d) Curet-Arana, M. C.; Emberger, G. A.; Broadbelt, L. J.; Snurr, R. Q. *J. Mol. Catal. A: Chem.* **2008**, *285*, 120–127. (e) Fukuzumi, S.; Kishi, T.; Kotani, H.; Lee, Y.-M.; Nam, W. *Nature Chem.* **2010**, *3*, 38–41.

(4) (a) Wieghardt, K.; Bossek, U.; Nuber, B.; Weiss, J.; Bonvoisin, J.; Corbella, M.; Vitols, S. E.; Girerd, J. J. *J. Am. Chem. Soc.* **1988**, *110*, 7398–7411. (b) Hage, R.; Iburg, J. E.; Kerschner, J.; Koek, J. H.; Lempers, E. L. M.; Martens, R. J.; Racheria, U. S.; Russell, S. W.; Swarthoff, T.; van Vliet, M. R. P.; Warnaar, J. B.; Wolf, L. V. D.; Krijnen, B. *Nature* **1994**, *369*, 637–639. (c) Quee-Smith, V. C.; DelPizzo, L.; Jureller, S. H.; Kerschner, J. L.; Hage, R. *Inorg. Chem.* **1996**, *35*, 6461–6465. (d) De Vos, D.; Bein, T. *Chem. Commun.* **1996**, 917–918.

(5) (a) Kanyo, Z. F.; Scolnick, L. R.; Ash, D. E.; Christianson, D. W. *Nature* **1996**, *383*, 554. (b) Wu, A. J.; Penner-Hahn, J. E.; Pecoraro, V. L. *Chem. Rev.* **2004**, *104*, 903. (c) Boelrijk, A. E. M.; Dismukes, G. C. *Inorg. Chem.* **2000**, *39*, 3020. (d) Pecoraro, V. L.; Baldwin, M. J.; Gelasco, A. *Chem. Rev.* **1994**, *94*, 807. (e) Jackson, T. A.; Brunold, T. C. *Acc. Chem. Res.* **2004**, *37*, 461.

(6) (a) Sauer, K. *Acc. Chem. Res.* **1980**, *13*, 249. (b) Yagi, M.; Kaneko, M. *Chem. Rev.* **2001**, *101*, 21. (c) Mukhopadhyay, S.; Mandal, S. K.; Bhaduri, S.; Armstrong, W. H. *Chem. Rev.* **2004**, *104*, 3981.

(7) (a) Zondervan, C.; Hage, R.; Feringa, B. L. *Chem. Commun.* **1997**, 419. (b) Berkessel, A.; Sklorz, C. *Tetrahedron Lett.* **1999**, *40*, 7965. (c) Gilbert, B. C.; Kamp, N. W. J.; Lindsay Smith, J. R.; Oakes, J. *J. Chem. Soc., Perkin Trans. 2* **1997**, 2161. (d) Barton, D. H. R.; Choi, S.-Y.; Hu, B.; Smith, J. A. *Tetrahedron* **1998**, *54*, 3367.

(8) (a) Lindsay Smith, J. R.; Shul'pin, G. B. *Tetrahedron Lett.* **1998**, *39*, 4909. (b) Shul'pin, G. B.; Suss-Fink, G.; Lindsay Smith, J. R. *Tetrahedron* **1999**, *55*, 5345. (c) Bennur, T. H.; Sabne, S.; Deshpande, S. S.; Srinivas, D.; Sivasanker, S. *J. Mol. Catal. A: Chem.* **2002**, *185*, 71.

(9) (a) Koek, J. H.; Kohlen, E. W. M. J.; Russell, S. W.; van der Wolf, L.; ter Steeg, P. F.; Hellemons, J. C. *Inorg. Chim. Acta* **1999**, *295*, 189–199. (b) Barker, J. E.; Ren, T. *Tetrahedron Lett.* **2004**, *45*, 4681.

(10) (a) Hage, R.; Lienke, A. *Angew. Chem., Int. Ed.* **2006**, *45*, 202. (b) Sibbons, K. F.; Shastri, K.; Watkinson, M. *Dalton Trans.* **2006**, 645.

(11) (a) Verrall, M. *Nature* **1994**, *369*, 511. (b) Verrall, M. *Nature* **1995**, *373*, 181.

(12) Gilbert, B. C.; Lindsay Smith, J. R.; Mairata I Payeras, A.; Oakes, J.; Prons I Prats, R. *J. Mol. Catal. A: Gen.* **2004**, *219*, 265–272.

(13) (a) De Vos, D. E.; Sels, B. F.; Reynaers, M.; Rao, Y. V. S.; Jacobs, P. A. *Tetrahedron Lett.* **1998**, *39*, 3221–3224. (b) Shul'pin, G. B.; Süss-Fink, G.; Shul'pina, L. S. *J. Mol. Catal. A.: Chem.* **2001**, *170*, 17–34. (c) Woitiski, C. B.; Kozlov, Y. N.; Mandelli, D.; Nizova, G. V.; Schuchardt, U.; Shul'pin, G. B. *J. Mol. Catal. A: Chem.* **2004**, *222*, 103–119. (d) Brinksma, J.; Schmieder, L.; van Vliet, G.; Boaron, R.; Hage, R.; De Vos, D. E.; Alsters, P. L.; Feringa, B. L. *Tetrahedron Lett.* **2002**, *43*, 2619–2622. (e) de Boer, J. W.; Brinksma, J.; Browne, W. R.; Meetsma, A.; Alsters, P. L.; Hage, R.; Feringa, B. L. *J. Am. Chem. Soc.* **2005**, *127*, 7990–7991.

(14) (a) de Boer, J. W.; Browne, W. R.; Brinksma, J.; Alsters, P. L.; Hage, R.; Feringa, B. L. *Inorg. Chem.* **2007**, *46*, 6353–6372. (b) de Boer, J. W.; Alsters, P. L.; Meetsma, A.; Hage, R.; Browne, W. R.; Feringa, B. L. *Dalton Trans.* **2008**, 6283–6295.

(15) (a) Shul'pin, G. B.; Kozlov, Y. N.; Kholuiskaya, S. N.; Plieva, M. I. *J. Mol. Catal. A: Chem.* **2009**, *299*, 77–87. (b) Zhou, S.; Chen, X.; Qian, C. *Chem. Phys. Lett.* **2010**, *488*, 44–49.

(16) (a) Herrmann, W. A.; Kratzer, R. M.; Blümel, J.; Friedrich, H. B.; Fischer, R. W.; Apperley, D. C.; Mink, J.; Berkesi, O. *J. Mol. Catal. A: Chem.* **1997**, *120*, 197. (b) Kolb, H. C.; VanNieuwenhze, M. S.; Sharpless, K. B. *Chem. Rev.* **1994**, *94*, 2483–2547.

(17) Schoenfeldt, N. J.; Korinda, A. W.; Notestein, J. M. *Chem. Commun.* **2010**, *46*, 1640–1642.

(18) Some relevant reviews: (a) Sheldon, R. A.; Wallau, W.; Arends, I. W. C. E.; Schuchardt, U. *Acc. Chem. Res.* **1998**, *31*, 485–493. (b) Choplin, A.; Quingnard, F. *Coord. Chem. Rev.* **1998**, *180*, 1679–1702. (c) Dusi, M.; Mallat, T.; Baiker, A. *Catal. Rev. Sci. Eng.* **2000**, *42*, 213–278. (d) Valkenberg, M. H.; Holderich, W. F. *Catal. Rev. Sci. Eng.* **2002**, *44*, 321–374. (e) Corma, A. *Catal. Rev. Sci. Eng.* **2004**, *46*, 369–417. (f) Notestein, J. M.; Katz, A. *Chem.—Eur. J.* **2006**, *12*, 3954–3965. (g) Augustine, R.; Tanielyan, S.; Anderson, S.; Gao, Y.; Goel, P.; Mahata, N.; Nair, I.; Reyes, C.; Yang, H.; Zsigmond, A. *ACS Symp. Ser.* **2004**, *880*, 15–28.

(19) (a) Madison, S. A.; Batal, D. J. (Lever Brothers Co.). U.S. Patent 5,284,944, 1994. (b) Searle, G. H.; Geue, R. J. *Aust. J. Chem.* **1984**, *37*, 959–970.

(20) Koek, J. H.; Russell, S. W.; van der Wolf, L.; Hage, R.; Warnaar, J. B.; Spek, A. L.; Kerschner, J.; DelPizzo, L. *J. Chem. Soc., Dalton Trans.* **1996**, 353–362.

(21) McKeen, J. C.; Yan, Y. S.; Davis, M. E. *Chem. Mater.* **2008**, *20*, 5122–5124.

(22) Thompson, A.; Attwood, D.; Gullikson, E.; Howells, M.; Kim, K.-J.; Kirz, J.; Kortright, J.; Lindau, I.; Liu, Y.; Pianetta, P.; Robinson, A.; Scofield, J.; Underwood, J.; Williams, G.; Winick, H. *X-Ray Data Booklet*, 2009.

(23) (a) Reed, C.; Lee, Y.-K.; Oyama, S. T. *J. Phys. Chem. B* **2006**, *110*, 4207–4216. (b) Tang, Q.; Gong, X.; Wu, C.; Chen, Y.; Borgna, A.; Yang, Y. *Catal. Commun.* **2009**, *10*, 1122–1126.

(24) Bunker, G. *Introduction to XAFS*; Cambridge University Press: Cambridge, UK, 2010.

(25) (a) Burch, R.; Cruise, N.; Gleeson, D.; Chi Tsang, S. *J. Mater. Chem.* **1998**, *8*, 227–231. (b) Stemmler, T. L.; Sossong, T. M.; Goldstein, J. I.; Ash, D. E.; Elgren, T. E.; Kurtz, D. M.; Penner-Hahn, J. E. *Biochemistry* **1997**, *36*, 9847–9858. (c) Caps, V.; Tsang, S. C. *Catal. Today* **2000**, *61*, 19–27.

(26) (a) Ravel, B.; Newville, M. *J. Synchrotron Radiat.* **2005**, *12*, 537–541. (b) Newville, M. *J. Synchrotron Radiat.* **2001**, *8*, 322–324.

(27) (a) Dimakis, N.; Farooqi, M. J.; Garza, E. S.; Bunker, G. *J. Chem. Phys.* **2008**, *128*, 115104−9. (b) Stern, E. A. *Phys. Rev. B: Condens. Matter* **1993**, *48*, 9825.

(28) Ravel, B. *J. Synchrotron Radiat.* **2001**, *8*, 314–316.

(29) (a) Kresse, G.; Furthmuller, J. *Phys. Rev. B* **1996**, *54*, 11169–11186. (b) Kresse, G.; Furthmuller, J. *Comput. Mater. Sci.* **1996**, *6*, 15–50.

(30) Vanderbilt, D. *Phys. Rev. B* **1990**, *41*, 7892–7895.

(31) Perdew, J. P.; Wang, Y. *Phys. Rev. B* **1992**, *45*, 13244–13249.

(32) Henkelman, G.; Arnaldsson, A.; Jonsson, H. *Comput. Mater. Sci.* **2006**, *36*, 354–360.

(33) Monkhorst, H. J.; Pack, J. D. *Phys. Rev. B* **1976**, *13*, 5188–5192.

(34) Wallar, B. J.; Lipscomb, J. D. *Chem. Rev.* **1996**, *96*, 2625–2657.

(35) Armarego, W. L. F.; Chai, C. L. L. *Purification of Laboratory Chemicals*, 5th ed.; Elsevier: Great Britain, 2003.

(36) Jeffrey, G. H.; Bassett, J.; Mendhem, J.; Denney, R. D. *Vogel's Textbook of Quantitative Chemical Analysis*, 5th ed.; Wiley: New York, 1989.

(37) (a) Liu, H.; Kondo, S.; Takeda, N.; Unno, M. *J. Am. Chem. Soc.* **2008**, *130*, 10074–10075. (b) Stock, C.; Heureux, N.; Browne, W. R.; Feringa, B. L. *Chem.—Eur. J.* **2008**, *14*, 3146–3153. (c) Prauzner-Bechcicki, J. S.; Godlewski, S.; Tekiel, A.; Cyganik, P.; Budzioch, J.; Szymonski, M. *J. Phys. Chem. C.* **2009**, *113*, 9309–9315. (d) Khashab, N. M.; Belowitch, M. E.; Trabolsi, A.; Friedman, D. C.; Valente, C.; Lau, Y.; Khatib, H.; Zink, J. I.; Stoddart, J. F. *Chem. Commun.* **2009**, 5371–5373. (e) Steckel, J.; Persky, N.; Martinez, C.; Barnes, C.; Fry, E.; Kulkarni, J.; Burgess, J.; Pacheo, R.; Stoll, S. *Nano Lett.* **2004**, *4*, 399.

(38) (a) Wieghardt, K.; Bossek, U.; Zsolnai, L.; Huttner, G.; Blondin, G.; Girerd, J.-J.; Babonneau, F. *J. Chem. Soc. D* **1987**, *9*, 651–653. (b) Schafer, K. O.; Bittl, R.; Zweygart, W.; Lendzian, F.; Haselhorst, G.; Weyhermuller, T.; Weighardt, K.; Lubitz, W. *J. Am. Chem. Soc.* **1998**, *120*, 13104–13120.

(39) (a) Lever, A. B. P. *Inorganic Electronic Spectroscopy*; Elsevier: New York, 1984. (b) Shepherd, R. E.; Hoq, M. F.; Hoblack, N.; Johnson, C. R. *Inorg. Chem.* **1984**, *23*, 3249–3252.

(40) Wieghardt, K.; Bossek, U.; Ventur, D.; Weiss, J. *J. Chem. Soc. D* **1985**, *6*, 347–349.
(41) Mas-Ballesté, R.; Que, L. *J. Am. Chem. Soc.* **2007**, *129*, 15964–15972.
(42) (a) De Vos, D. E.; de Wildeman, S.; Sels, B. F.; Grobet, P. J.; Jacobs, P. A. *Angew. Chem., Int. Ed.* **1999**, *38*, 980–983. (b) Lazarys, L. L.; Brutchey, R. L. *Dalton Trans.* **2010**, *39*, 7888–7890. (c) Severeyns, A.; De Vos, D. E.; Jacobs, P. A. *Green Chem.* **2002**, *4*, 380–384. (d) Severeyns, A.; De Vos, D. E.; Fiermans, L.; Verpoort, F.; Grobet, P. J.; Jacobs, P. A. *Angew. Chem., Int. Ed.* **2001**, *40*, 586–589. (e) Bataille, C. J.; Donohoe, T. J. *Chem. Soc. Rev.* **2011**, *40*, 114–128.
(43) (a) Sibbons, K. F.; Shastri, K.; Watkinson, M. *Dalton Trans.* **2006**, 645–661. (b) Matsubara, S.; Takai, K.; Nozaki, H. *Bull. Chem. Soc. Jpn.* **1983**, *56*, 2029–2032.
(44) Signorella, S.; Rompel, A.; Buldt-Karentzopoulos, K.; Krebs, B.; Pecoraro, V. L.; Tuchagues, J. P. *Inorg. Chem.* **2007**, *46*, 10864–10868.
(45) Schoenfeldt, N. J.; Notestein, J. M. *ACS Catal.* **2011** in press, http://pubs.acs.org/doi/abs/10.1021/cs200353x.
(46) Notestein, J. M.; Solovyov, A.; Andrini, L. R.; Requejo, F. G.; Katz, A.; Iglesia, E. *J. Am. Chem. Soc.* **2007**, *129*, 15585–15595.
(47) (a) Que, L.; Tolman, W. B. *Nature* **2008**, *455*, 333–340. (b) Kwong, H. K.; Lo, P. K.; Lau, K. C.; Lau, T. C. *Chem. Commun.* **2011**, *47*, 4273–4275. (c) Company, A.; Prat, I.; Frisch, J. R.; Mas-Balleste, R.; Guell, M.; Juhasz, G.; Ribas, X.; Munck, E.; Luis, J. M.; Que, L.; Costas, M. *Chem.—Eur. J.* **2011**, *17*, 1622–1634. (d) Cheung, W. H.; Yu, W. Y.; Yip, W. P.; Zhu, N. Y.; Che, C. M. *J. Org. Chem.* **2002**, *67*, 7716–7723.
(48) Grimme, S.; Antony, J.; Ehrlich, S.; Krieg, H. *J. Chem. Phys.* **2010**, 132.